Mammograms calcifications segmentation based on band-pass Fourier filtering and adaptive statistical thresholding

Elizabeth López Meléndez[1] and Gonzalo Urcid[2]

[1,2] Instituto Nacional de Astrofísica, Óptica y Electrónica (INAOE)
Luis Enrique Erro, No. 1, Tonanzintla, 72840, Puebla, México

[2]Corresponding Author Email: gurcid@inaoep.mx

Abstract

To segment calcifications and microcalcifications in digital mammograms we introduce a Butterworth band-pass filter in the Fourier domain to enhance edges of objects in order to obtain their shapes. The proposed filter is compared to two edge finders, the difference of Gaussians and the Laplacian of a Gaussian. Also a comparison of the behavior of these filters is given in both domains. Once the edges are enhanced, a median filter is applied to remove fibroglandular tissue after which a gamma correction is performed to increase the contrast of the pathologies to be segmented. Image binarization is achieved with Otsu's global thresholding method by considering the image of its local variances and compared with Sauvola's thresholding method. The final segmented image is the result of applying a sequence of morphological operations such as closing and region filling. Several illustrative examples taken from a clinical database are provided to demonstrate the capability of the proposed segmentation technique.

Keywords: adaptive thresholding, difference of Gaussians, Butterworth frequency filters, Laplacian of Gaussian, mammograms segmentation

1. Introduction

Worldwide, breast cancer is the first cause of death as reported by public hospitals [23]. In order to obtain an early diagnosis of breast cancer, different techniques of breast imaging are commonly applied such as ultrasound, mammography, computerized tomography, magnetic resonance imaging, or thermography imagery [2, 4,22]. However, due to substantial differences in cost of each imaging modality, the most used and accessible technique in public hospitals is the acquisition of X-ray mammograms needed specifically for microcalcifications.

Microcalcifications detection in digitized or digital acquired mammograms has been tackled since 1993 with different approaches based on various mathematical models such as the difference of Gaussians [9, 10,11,12,15], mathematical morphology [3], and wavelet transforms [1,8,13,18], to name a few. Recently, Rizzi [19] presented a general review and comparison between different detection methods of tumors, calcifications, and microcalcifications.

In this paper, our attention focuses only in the detection of calcifications or microcalcifications. Specifically, we propose a Butterworth band-pass filter in the Fourier domain and, for comparison purposes, we also treat the *Difference of Gaussians* (DoG) [5] as well as the *Laplacian of a Gaussian* (LoG) [7], to find object edges after filtering in the Fourier frequency using the corresponding spatial models. The resulting edge image based on the aforementioned filters is enhanced by applying first a median filter followed by a gamma correction to reduce background noise as well as to increase the contrast of object borders. The next step performs a binarization operation using local and global statistics with Otsu's and Sauvola's thresholding techniques to obtain the desired binary object regions. Final image segmentation is achieved with the morphological closing and filling by reconstruction operations with a suitable structuring element.
The paper is organized as follows: Section 2 explains in some detail the mathematical background needed to understand the previously mentioned methods used for the segmentation of calcifications or microcalcifications. We provide an illustrative example that compares the proposed Butterworth band-pass filter against DoG and LoG, including our adaptive statistical thresholding proposed technique versus Sauvola's thresholding technique. Section 3 presents several image post-processing steps required before segmentation. The overall segmentation algorithm based on Fourier edge finders is presented in pseudocode format. Section 4 shows several representative examples of calcifications and microcalcifications detection in digital mammograms and a technical discussion is given of adaptive thresholding values as well as the predictive validity of our proposal in terms of a confusion matrix. Finally, in Section 5, the conclusions to the present research are commented.

2. Problem Description and Mathematical Background

The problem we are dealing with is to find calcifications and microcalcifications in X-ray digtial mammograms. To find objects of interest in a given digital image it is common to device a procedure that implements some kind of *separation* or *segmentation* of specific objects from other less important objects such as, for example, surrounding tissue or other physiological structures. In the present work, we consider local regions selected from the whole mammogram. Any of these image regions is known as *region of interest* (ROI) considered as small window of 256×256 pixels, equivalent to an image area of 12.8 mm $\times$ 12.8 mm =163.84 mm^2. When an image is segmented, it is possible to distinguish the objects of interest from the image background by partitioning the image in several subimages or regions that satisfy certain conditions as explain elsewhere [11, 22].

2.1 Spatial edge finders

The first edge detector used is the difference of Gaussians, where it is consider that a Gaussian function is taken with zero mean and finite standard deviation σ. Eq. 1 shows the expression of the DoG filter in the spatial domain, where $\sigma_1 > \sigma_2$. Laplacian filters are derivative filters used to find zones of rapid intensity changes (edges) in images. Since derivative filters are very sensitive to noise, it is common to smooth the image (e.g., using a Gaussian filter) before applying the Laplacian. The Laplacian of Gaussian or LoG operator takes the second coordinate derivatives of the image. If the image contains uniform areas, the LoG will give zero. Wherever a change occurs in a given region, the LoG will give a positive response on the

dark side and a negative response on the bright side. The expression of the LoG spatial filter is given in Eq.2. Recall that the 2D Laplacian operator is defined by, $\nabla f(x, y) = f_{xx} + f_{yy}$.

$$\text{DoG}(x, y; \sigma_1, \sigma_2) = e^{-\left(\frac{x^2+y^2}{2\sigma_1^2}\right)} - e^{-\left(\frac{x^2+y^2}{2\sigma_2^2}\right)}, \tag{1}$$

$$\text{LoG}(x, y; \sigma) = \nabla e^{-\left(\frac{x^2+y^2}{2\sigma^2}\right)} = \frac{2\sigma^2 - x^2 - y^2}{\sigma^4} e^{-\left(\frac{x^2+y^2}{2\sigma^2}\right)}. \tag{2}$$

2.2 Frequency Edge Finders

The two dimensional continuous Fourier transform is defined by,

$$F(u, v) = \mathcal{F}\{f(x, y)\} = \int_{-\infty}^{\infty} \int_{-\infty}^{\infty} f(x, y) e^{-i2\pi(ux+vy)} dx dy \tag{3}$$

and the corresponding filter expressions in the Fourier domain of Eqs. (1) and (2) are given by,

$$H_{\text{DoG}}(u, v; \sigma_1, \sigma_2) = \mathcal{F}\{\text{DoG}(x, y; \sigma_1, \sigma_2)\} = 2\pi \left[\sigma_1^2 e^{-2\pi^2\sigma_1^2(u^2+v^2)} - \sigma_2^2 e^{-2\pi^2\sigma_2^2(u^2+v^2)} \right], \tag{4}$$

$$H_{\text{LoG}}(u, v; \sigma) = \mathcal{F}\{\text{LoG}(x, y; \sigma)\} = 8\pi^3\sigma^2(u^2 + v^2) e^{-2\pi^2\sigma^2(u^2+v^2)}. \tag{5}$$

The two dimensional discrete Fourier transform (DFT) is given by,

$$F(u, v) = \mathcal{F}\{f(x, y)\} = \sum_{x=0}^{M-1} \sum_{y=0}^{N-1} f(x, y) e^{-i2\pi(ux/M+vy/N)}, \tag{6}$$

where, $f(x,y)$ is the input image of size $M \times N$ pixels and $u = 0, 1, ..., M-1$, $v = 0, 1, ..., N-1$ are ranges of a finite number of frequency samples. Before filtering, $f(x,y)$ is multiplied by $(-1)^{(x+y)}$ to center the discrete transform which is computed with a *fast Fourier transform* (FFT) algorithm. In a similar way as the spatial edge finders, we demonstrate that Fourier based edge detectors are able to find local discontinuities of intensity in a given mammogram's ROI. The selected ROI is then processed with a Butterworth band-pass filter which will be defined later. The resulting spatial filtered image, denoted by $g(x,y)$, is computed as follows,

$$g(x, y) = \mathcal{F}^{-1}\{F(u, v)H(u, v)\}, \tag{7}$$

where, F^{-1} is the *inverse discrete Fourier transform* (IDFT), $F(u,v)$ is the (DFT) of the input image $f(x, y)$, and $H(u,v)$ is a Butterworth band-pass filter. For numerical computation, functions F, H, and g are matrices of size $M \times N$. Since low frequencies are generated by spatial components whose intensities vary slowly and high frequencies correspond to abrupt transitions in intensities, such as edges or noise, the frequency filter is designed to extract object edges by modifying the Fourier spectrum of the input image. An *n-th* order *Butterworth band-pass* (BBP) frequency filter is defined as follows,

$$H_{BBP}(u,v) = \frac{1}{1 + \left[\left(D^2(u,v) - D_0^2\right)/WD(u,v)\right]^{2n}}, \tag{8}$$

where, $D(u,v) = \sqrt{(u - M/2)^2 + (v - N/2)^2}$, is the Euclidean distance between (u,v) and the filter center $(M/2, N/2)$, $W = D_H - D_L$ is the filter bandwidth, and $D_0 = (D_H + D_L)/2$ is the cutoff frequency.

2.3 Filter Design Parameters

The relation between the spatial sampling Δx and the frequency intervals Δu in the discrete frequency domain is $\Delta u = 1/M\Delta x$. For our study, since we have $M = N = 256$ pixels image samples and a digitizer spatial resolution of $\Delta x = 50$ μm = 0.05 mm, then $\Delta u = 1/256(0.05) = 0.078125$ mm^{-1}. The spacing values are the same, respectively, for the Δy and Δv sampling intervals. Because it is required to filter out low frequencies for relatively extended objects such as fibroglandular tissue as well as high frequencies produced by tinny objects or noise that can trigger false positives, we consider calcifications or clusters of microcalcifications with sizes between 0.34 mm and 2.55 mm [6] that correspond to the discrete spatial frequencies of 2.941 mm^{-1} and 0.392 mm^{-1}, respectively. According to our frequency spacing value, the nearest values we can have for the high cutoff frequency (D_H) and the low cutoff frequency (D_L) are 2.891 mm^{-1} and 0.391 mm^{-1}, which in turn correspond to pixel values of 37 and 5 in the frequency domain. These last values are the limiting cutoff frequencies of the proposed Butterworth band-pass filter. Therefore, the width of the frequency band is $W = 32$ and $D_0 = 21$; also, we choose $n = 3$ for the order of the filter as a compromise to balance the filter response between an ideal and a Gaussian band-pass filter. Note that pixel values in the frequency domain depend on the number of samples of the image region of interest; thus, for a larger number of samples the values of W and D_0 will increase proportionally. As a physical reference we write between parenthesis the area (in mm^2) or lateral distance (in mm) associated with image parameters.

In Fig. 1 we show a test ROI filtered with Eqs. (1), (2), and (8); for the DoG filter, the parameter values are set to $\sigma_1 = 2$ and $\sigma_2 = 1.7$, and associated square masks of 11×11 pixels (0.302 mm^2) and 5×5 pixels (0.062 mm^2), respectively. Similarly, the LoG standard deviation value is set to $\sigma = 2$ and associated mask of 11×11 pixels (0.302 mm^2). Note that the corresponding parameter values of the Butterworth band-pass filter are the ones computed before.
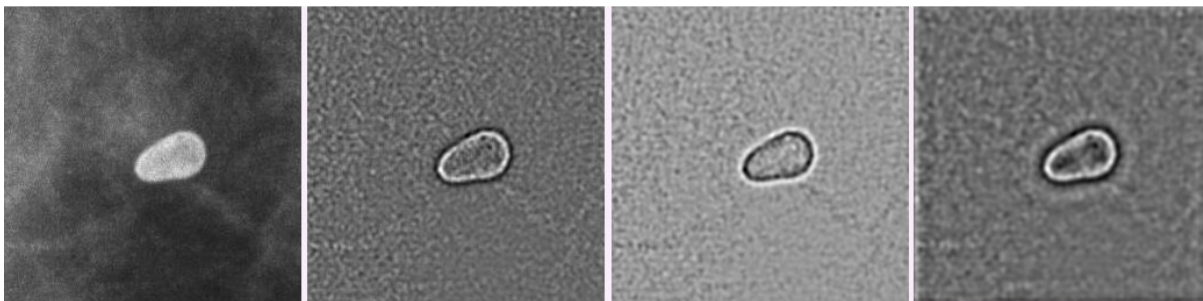

Fig. 1. From left to right: image ROI, DoG filtered ROI, LoG filtered ROI, and BBP filtered ROI.

On the left of Fig. 2, the profiles of the edge finder filters as graphed in the frequency domain display a similar behavior through the band-pass. The profiles shown to the right of the same figure are the spatial versions of the corresponding frequency filters. Note that the DoG and BBP filters have a similar shape, whereas the LoG filter has a mirror shape of DoG with respect to the *x* axis, suggesting inverted filtering.
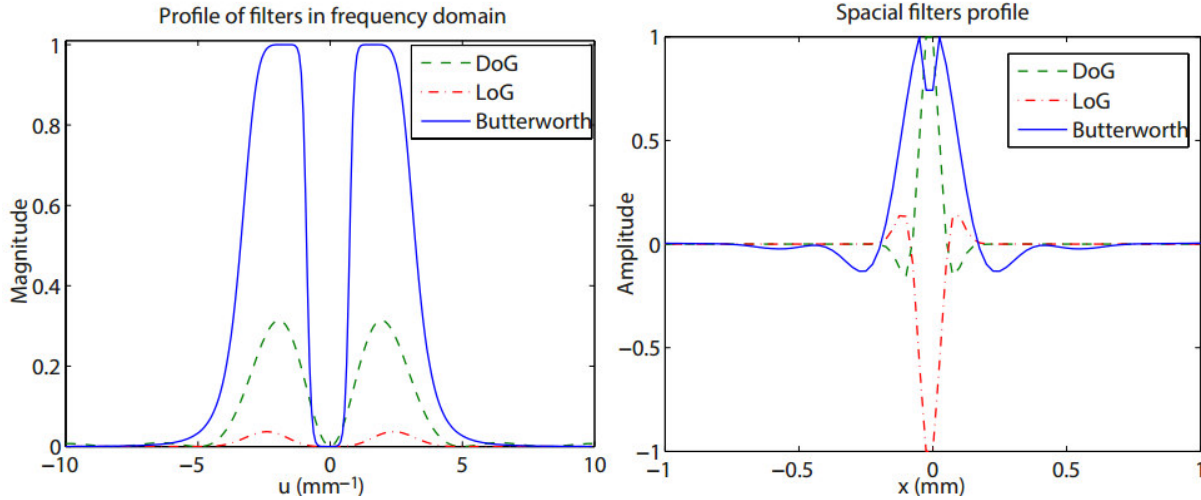
Fig. 2. Left, frequency domain filter profiles along *u* ; right, spatial domain filter profiles along *x*.

3. Post-processing and Segmentation

The resulting image using any of the edge detectors discussed is enhanced with a median filter of size 3×3 pixels (0.022 mm^2) to reduce the noise in the fibroglandular tissue and a gamma correction of value 1.25 is applied to emphasize calcification edges by lowering darker grayscale values and augmenting brighter ones. The next step consists in thresholding the previous image and binarize it using statistical moments. We recall that the mean and variance, given in Eqs. (10) and (11), can be defined globally (*G* label) on the entire image or locally (*L* label) over finite image subregions. Thus, we have that,

$$m_G = \frac{1}{MN} \sum_{x=0}^{M-1} \sum_{y=0}^{N-1} f(x,y) \qquad ; \quad \sigma_G^2 = \frac{1}{MN} \sum_{x=0}^{M-1} \sum_{y=0}^{N-1} [f(x,y) - m_G]^2, \tag{10}$$

$$m_L(x,y) = \frac{1}{|R_{xy}|} \sum_{(r,c) \in R_{xy}} f(r,c) \quad ; \quad \sigma_L^2 = \frac{1}{|R_{xy}|} \sum_{(r,c) \in R_{xy}} [f(r,c) - m_L(x,y)]^2, \tag{11}$$

where, R_{xy} is a neighborhood centered at (x,y) of size $k \times k$ pixels. In the case of the mammograms ROI's tested here, the corresponding binary images are obtained using Eq. (12) with a neighborhood R_{xy} of size 5×5 pixels (0.062 mm^2), and $\alpha > 0$ is a scaling factor that relates the local and global variances.

$$B(x,y) = \begin{cases} 0 & \text{if } \sigma_L^2(x,y) < \alpha \sigma_G^2, \\ 1 & \text{otherwise.} \end{cases} \tag{12}$$

The binary morphological operations [21] used to connect object edges and fill the corresponding regions are two chained operations. First, a morphological closing operation is applied followed by a morphological region filling operation based on geodesic reconstruction. In our case, the structuring element S_7 used in both operations is a disk of radius 7 pixels (0.35 mm). Specifically, the morphological closing operation is computed by,

$$I = B \bullet S_7 = (B \oplus S_7) \ominus S_7, \tag{13}$$

and the morphological region filling operation is given by the expression shown in Eq. (15), where $I(x,y)$ is the input binary image to fill, $M(x,y)$ is the *marker image* built from the image delimiting frame, I^c is the complement of the input image, and $D_{I^c}^k(M)$ is the k-th geodesic morphological dilation of M bounded by I^c.

$$M(x,y) = \begin{cases} 1 - I(x,y) & \text{if } (x,y) \text{ is on the border of } I \\ 0 & \text{otherwise} \end{cases},$$

$$D_{I^c}^k(M) = D_{I^c}^1(D_{I^c}^{k-1}(M)) \quad \text{where,} \quad D_{I^c}^1(M) = (M \oplus S_7) \cap I^c \text{ and } D_{I^c}^0(M) = M, \quad (14)$$

$$\Rightarrow \quad B_f = (R_{I^c}^D(M))^c \cap I^c. \quad (15)$$

In Fig. 3 we show the post-processing and segmentation of a ROI containing eggshell calcifications with the method proposed.

Fig. 3. Left, eggshell calcifications image (ROI). Center, binarized calcification image. Right, resulting ROI after morphological closing and filling operations.

An alternative binarization method based on local statistics that provides an adaptive local threshold appears in Sauvola [20], its expression is given below,

$$B_S(x,y) = m_L(x,y)\left[1 + \alpha_S\left(\frac{\sigma_L(x,y)}{\sigma_{L\max}} - 1\right)\right], \quad (16)$$

where, σ_{Lmax} is the maximum of the local standard deviations and $\alpha_S \in [0,1]$ is a threshold factor; to compute B_S a mask R_{xy} of size 5×5 pixels (0.122 mm^2) is used. A comparison between Sauvola's thresholding method and ours (see Eq. (12)), applied to a mammogram ROI, is shown in Figs. 4 and 5, respectively, for the three types of filters used. It can be observed that the superimposed border of the dystrophic calcification is best approximated by the proposed technique. The contrast correction value used for to enhanced the mammogram ROI is $\gamma = 1.25$ for Sauvola's method and $\gamma = 2$ for our technique.
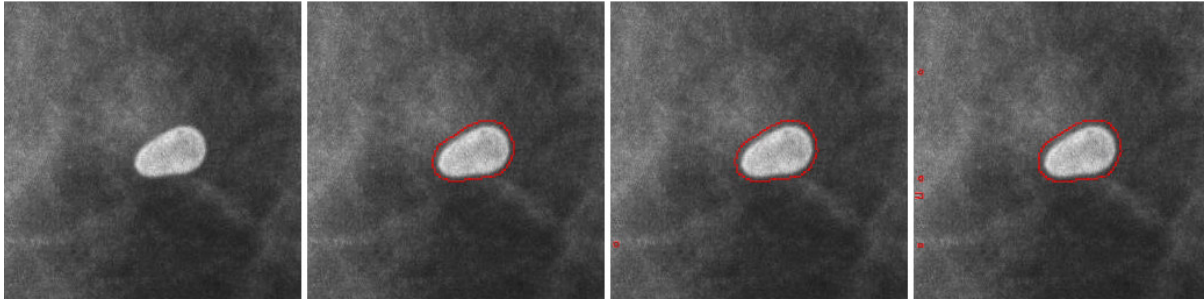
Fig. 4. Results using Sauvola's method. From left to right, dystrophic calcification image (ROI), DoG based segmentation, LoG based segmentation, and BBP based segmentation.
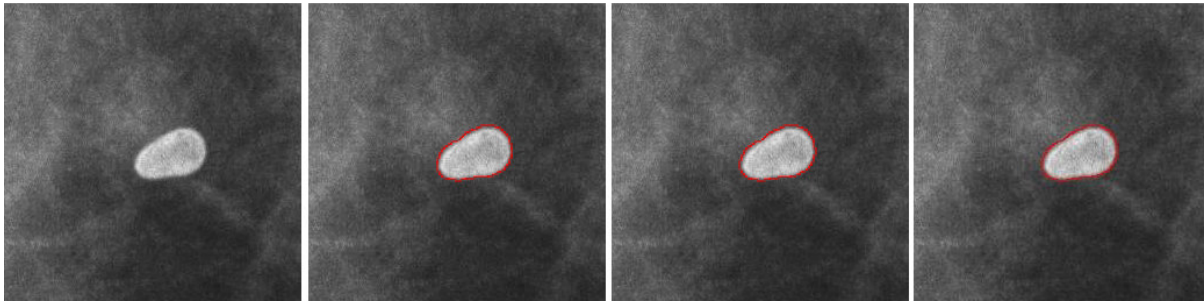

Fig. 5. Adaptive local & global statistics method proposed. From left to right, dystrophic calcification image (ROI), DoG segmented image, LoG segmented image, and BBP segmented image.

In Algorithm FEDBS, the necessary segmentation steps are shown in pseudo-code format. Note that meanwhile Sauvola's thresholding function makes use only of local statistics, our method establishes a thresholding criterion that compares local variances to the global variance of a ROI based on Otsu's method to get the alpha factor.

Algorithm: Frequency Edge Detector Based Segmentation (FEDBS)

Input parameters: $[D_0, W, n, \alpha, S_7]$

Image filtering

Select mammogram region of interest: $ROI \leftarrow Cropped\ Mammogram$
  Case: DoG filter
      Compute DoG filter with $\sigma_1 = 2, \sigma_2 = 1.7$: $FI \leftarrow DoG(ROI, \sigma_1, \sigma_2)$
  Case: LoG filter
      Compute LoG filter with $\sigma = 2$: $FI \leftarrow LoG(ROI, \sigma)$
  Case: Fourier filter
      Compute 2D fast Fourier transform: $FROI \leftarrow FFT(ROI)$
      Specify band-pass frequency filter $D_0 = 21$, $W = 32, n = 3$: $H \leftarrow H_{BBP}(FROI, D_0, W, n)$
      Get filtered image by 2D inverse fast Fourier transform: $FI \leftarrow IFFT(FROI \cdot H)$
      (the binary operation $\cdot$ denotes elementwise matrix multiplication)

Post-processing

Reduce background noise: $FI \leftarrow Median\ Filter(FI)$

Enhance contrast: $FI \leftarrow Gamma\ Correction(FI, \gamma)$

Image segmentation

Compute global and local variances $(k = 5): \{\sigma_L^2, \sigma_G^2\} \leftarrow Statistics(FI)$

Turn pixel on if $\sigma_L^2(x, y) \geq \alpha\sigma_G^2: B \leftarrow Binarize(FI, \alpha, \sigma_G^2, \sigma_L^2)$

Close objects with a disk of radius $7: I \leftarrow Morphological\ Closing(B, S_7)$

Get final segmented objects of ROI: $B_f \leftarrow Region\ Filling\ (I, S_7)$

4. Image Segmentation Examples

In this research, we tested digital mammograms with a spatial resolution of $50\ \mu m$ per pixel. The mammograms were taken from a clinical database acquired at the Radiology Department of the University Hospital of Puebla city [14] in Mexico. The radiological equipment used to obtain the mammograms consisted of a *Planmed Sophie Classic* breast image capturing device [17] consisting of an X-ray source controller, an *AGFA* [16] *CRMM3.0 Mammo plate* with size of 29×26 cm, and an *AGFA CR35-X Digitizer*. We remark that the AGFA plate is dedicated for diagnostic mammography applications. Representative ROI's of calcifications and microcalcifications images contain different shapes such as popcorn formed calcifications of high intensity, eggshells that look translucent with enhanced edges, and dystrophic translucent calcifications with irregular shapes. Also, punctuate microcalcifications are small concentrations of calcium that can be seen as very bright spots on the fibroglandular tissue (background).

In Table 1, the threshold values used for Sauvola's method (α_S) as well as in the proposed method (α) are listed in every tested case for each filter used. In the same table we observe that the α values depend on the low or high contrast of the mammogram's ROI; when the contrast is higher the alpha value decreases and for lower contrast the alpha value increases.

Table 1. Adaptive threshold values obtained with Sauvola's method and the proposed method.

Figure No. and Type of calcification	DoG		LoG		BBP	
	α_S	α	α_S	α	α_S	α
4. Dystrophic	0.65	6.11	0.62	5.67	0.57	4.17
5. Deformed popcorn	0.29	1.38	0.34	1.95	0.27	1.20
6. Round and punctuate	0.97	9.00	0.94	9.40	0.96	5.65
7. Mixed calcifications	0.87	5.01	0.91	5.21	0.78	5.45
8. Eggshell	0.63	7.34	0.61	7.03	0.57	6.06
9. Eggshell and round	0.73	5.86	0.71	4.71	0.75	4.45

The different ROI's were processed using the three different edge finders described in Section 2. Figures 6 to 10, display a panel of each example image composed of the mammogram's region of interest and the segmentation of detected objects for each filtering method. Since some details cannot be very well appreciated, instead of performing a masking operation with the whole binary image the corresponding binary edges are superimposed (in red) as a visual aid on the mammogram's ROI. We point out that only the results of our segmentation method are given since the results obtained with Sauvola's method are coarser.
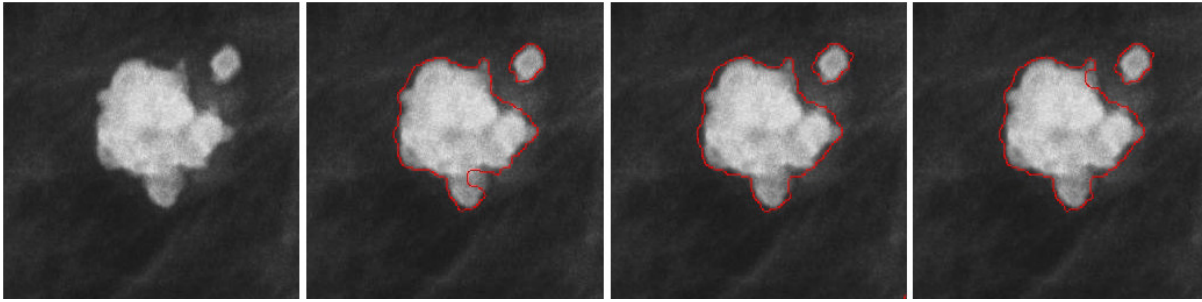
Fig. 6. Adaptive local & global statistics thresholding method proposed. From left to right, deformed popcorn calcification image (ROI), DoG segmented image, LoG segmented image, and BBP segmented image.
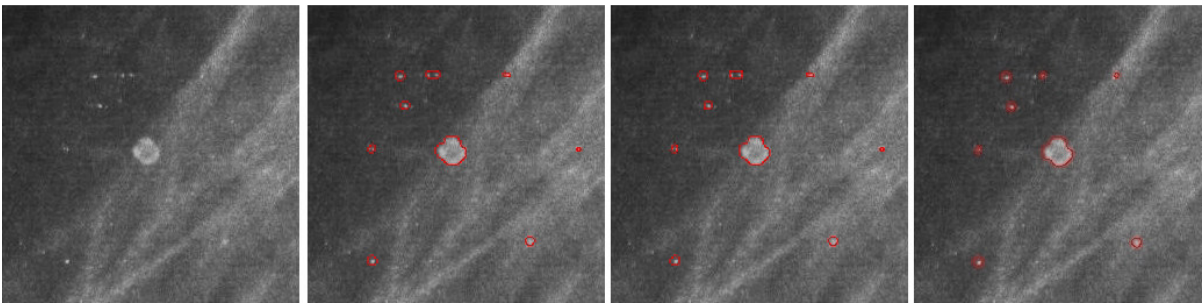

Fig. 7. Adaptive local & global statistics thresholding method proposed. From left to right, punctuate and eggshell calcifications image (ROI), DoG segmented image, LoG segmented image, and BBP segmented image.
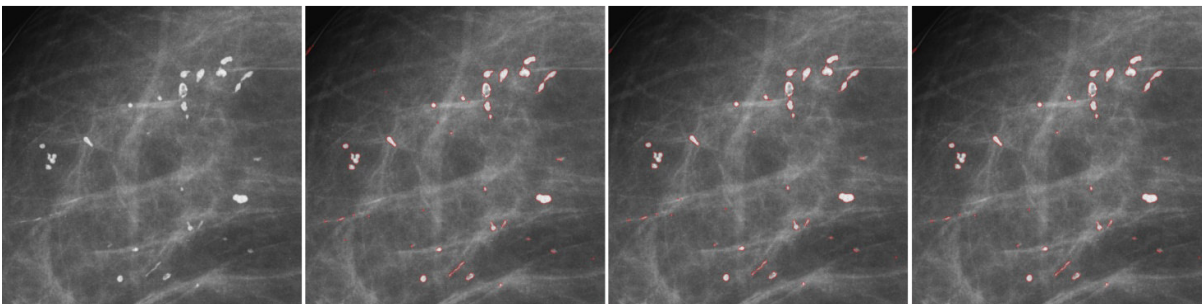

Fig. 8. Adaptive local & global statistics thresholding method proposed. From left to right, different types of calcifications image (ROI), DoG segmented image, LoG segmented image, and BBP segmented image.
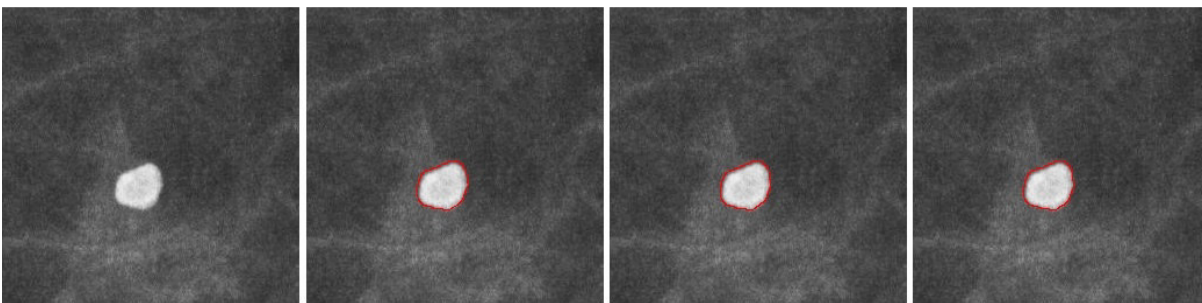

Fig. 9. Adaptive local & global statistics thresholding method proposed. From left to right, eggshell calcification image (ROI), DoG segmented image, LoG segmented image, and BBP segmented image.
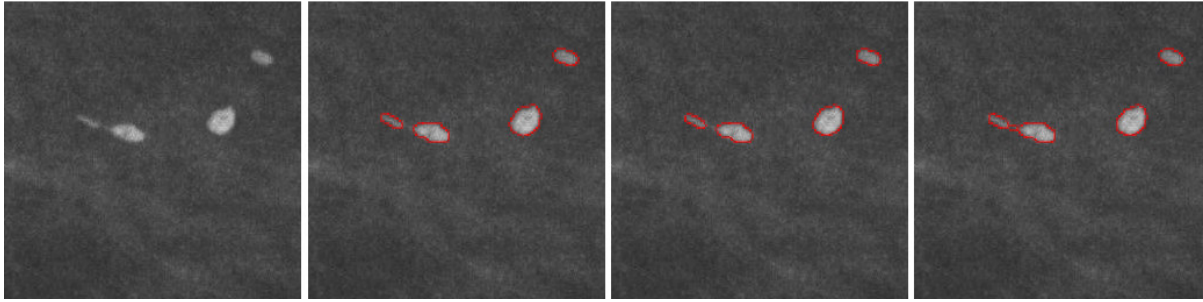
Fig. 10. Adaptive local & global statistics thresholding method proposed. From left to right first row, eggshell and round calcifications image (ROI), DoG segmented image, LoG segmented image, and BBP segmented image.

In the clinical medical profession it is common practice to evaluate the performance of a system using a confusion matrix that contains information about actual and predicted classifications realized by a pattern recognition system [10]. The entries of a confusion matrix are given in Table 2.

Table 2. Entries of a 2 × 2 confusion matrix.

Positive test	True positive *TP*	False positive *FP*
Negative test	False negative *FN*	True negative *TN*
Total	*TP + FN*	*FP + TN*

The confusion matrix has four entries which are, the number *TP* of correctly detected objects (calcifications or microcalcifications) that a test group sample gives positive, the number *TN* of incorrectly detected objects that a test group sample gives negative, the number *FP* of correctly detected objects classified erroneusly (negative), and the number *FN* of incorrectly detected objects classified as positive. The confusion matrix helps us to find the *true positive rate* (*TPR*), also known as *sensitivity*, which refers to the proportion of objects that give positive test results, and the *true negative rate* (*TNR*), also known as *specificity*, which refers to the proportion of objects that give negative test results. Equations (17) and (18) gives these proportions,

$$TPR = \frac{TP}{TP + FN},$$ (17)

$$TNR = \frac{TN}{TN + FP}.$$ (18)

To estimate the rates *TPR* and *TNR*, we took 20 mammogram hand-marked ROI's from a total of 25 processed mammograms. The numerical values found for the three frequency domain based segmentation methods discussed previously are given in Table 3.

Table 3. *TPR* and *TNR* for the spatial and frequency domain filters.

Microcalcifications Segmentation		
	TPR	*TNR*
DoG	0.9823	0.9699
LoG	0.9798	0.9796
BBP	0.9814	0.9870

In Figs. 11 and 12, we show a calcifications ROI as an example of the difference between a hand-marked image and the resulting segmented image. It can be observed in Fig. 11, that the hand-marked calcification ROI is similar to the region obtained based on Fourier BBP filtering. Also, in Fig. 12, our method is capable of finding small regions when compared with the corresponding hand-marked image.
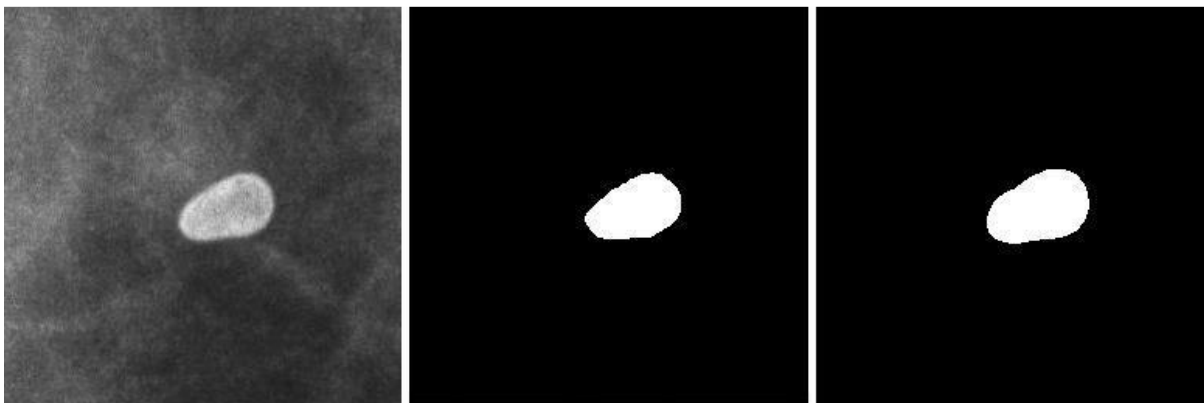
Fig. 11. From left to right, dystrophic calcification image (ROI), hand-marked segmentation, and BBP segmented image.
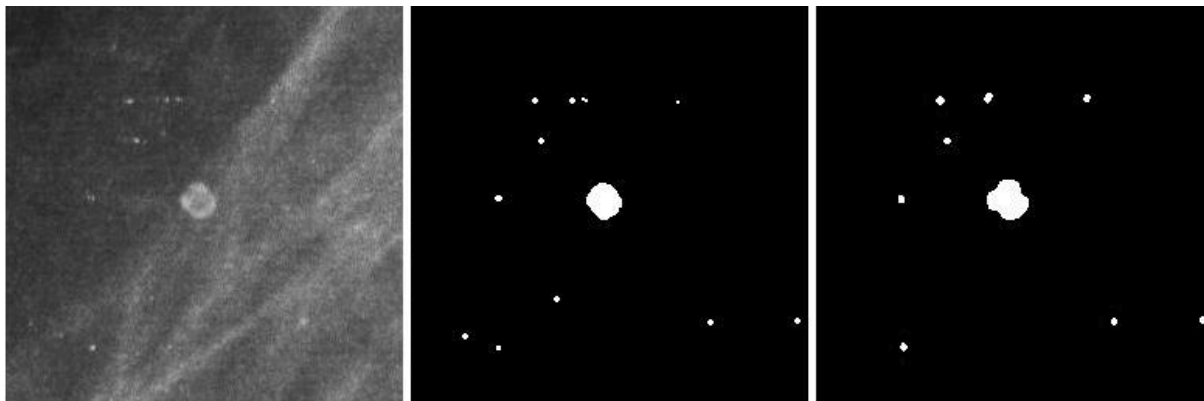
Fig. 12. From left to right, eggshell and round calcifications image (ROI), hand-marked segmentation, and BBP segmented image

4. Conclusions

In this paper, we proposed a Butterworth band-pass filter in the Fourier domain as an edge finder technique for the segmentation of calcifications and microcalcifications in digital mammograms that is competitive as other well known spatial edge finders. Note that the BBP filter allows tunable control over the frequencies within its bandwidth by assigning properly the high and low cutoff frequencies as well as the slope rate determined by its order. By applying a BBP filter, the fibroglandular tissue (background) is easier to remove and simultaneously it enhances the edges of objects (foreground). Otsu's thresholding method is used to

obtain a global threshold based on the local variances by windowing the filtered image, delivering a better contrast between foreground and background. Our approach to segmentation is compactly coded in Algorithm FEDBS. A test example is included to compare the results obtained with the DoG, LoG, and BBP filters. Also, several illustrative clinical examples of representative mammograms containing calcifications or microcalcifications shapes are displayed. To validate our results for each filter type, we compute a confusion matrix giving high sensitivity and specificity with respect to the samples considered. Future work contemplates the design of an interactive or automatic pathology classification system based on the BIRADS (*Breast Imaging Reporting and Data System*) standard [22].

Acknowledgments

References

[1] Abubaker A. A. (2015). Automatic microcalcification detection using wavelet transform, *International Journal of Computer Theory and Engineering*, 7(1), 40-45.

[2] AGFA healthcare. (2015). www.agfahealthcare.com /global/ en/main/landing/ index.jsp. Germany

[3] Betal D., Roberts N., & Whitehouse G. (1997). Segmentation and numerical analysis of microcalcifications on mammograms using mathematical morphology, *The British Journal of Radiology*, 70(837), 903-917.

[4] Breast imaging (2015): http://www.cancer.org/acs/groups/cid/documents/webcontent/acspc-033538-pdf.pdf

[5] Bundy A. & Wallen L. (1984). Difference of Gaussians, *Catalogue of Artificial Intelligence Tools*, Springer Symbolic Computation Series, 30.

[6] Cardeñosa G. (2008). *Breast Imaging Companion.* (3rd ed.). Lippincott Williams & Wilkins, Philadelphia, PA.

[7] Chen J. S., Huertas A., & Medioni G. (1987). Fast convolution with Laplacian-of-Gaussian masks, *IEEE Transactions on Pattern Analysis and Machine Intelligence*, 9, 584-590.

[8] Cheng H. D. & Wang J. (2003). Fuzzy logic and scale space approach to microcalcification detection, *Proceedings of IEEE: International Conference on Acoustics, Speech, and Signal Processing*, 2, II-345.

[9] Dengler J., Behrens S., & Desaga J. (1993). Segmentation of microcalcifications in mammograms, *IEEE Transactions on Medical Imaging*, 12, 634-642.

[10] Fawcett T. (2004). ROC graphs: Notes and practical considerations for researchers, *Machine learning*, 31, 1-38.

 [11] Gonzalez, R. & Woods, R. E. (2009). *Digital Image Processing*, (3rd ed.).Pearson, Prentice Hall, Upper Saddle River, NJ.

[12] Gur D., Zheng B., & Chang Y. (1997). Computerized detection of masses and microcalcifications in digital mammograms, US Patent 5,627,907.

[13] Hamad N. B., Taouil K., & Bouhlel M. S. (2013). Mammographic microcalcifications detection using discrete wavelet transform, *International Journal of Computer Applications*, 64, 21.

[14] Hospital Universitario de Puebla. (2015). www.buap.mx/portal$_{-}$pprd/wb/hup/hup, Puebla, México.

[15] López-Meléndez E., Lara-Rodríguez L., et al. (2012). BICAD: Breast image computer aided diagnosis for standard BIRADS 1 and 2 in calcifications, *Proceedings of IEEE: 22nd International Conference on Electrical Communications and Computers*, 190-196.

[16] López-Meléndez E., Lara-Rodríguez L., & Urcid G. (2015). Fourier-based segmentation of microcalcifications in mammograms. *Proceedings of SPIE: Applications of Digital Image Processing XXXVIII*, 9599, 95992N1-10.

[17] Planmed Oy Company, (2015). [Online] available: http: //www.planmed.com /Mammography /Analog-mammography /~Planmed-Sophie -Classic/. Finland.

[18] Ping W. et al. (2008). A method of detection microcalcifications in mammograms using wavelets and adaptive thresholds, *Proceedings of IEEE: 2nd International Conference on Bioinformatics and Biomedical Engineering*, 2361-2364.

[19] Rizzi M., D'Aloia M., & Castagnolo B. (2012). Review: Health care CAD systems for breast microcalcification cluster detection, *Journal of Medical and Biological Engineering*, 32(3), 147-156.

[20] Sauvola J. & Pietikäinen M. (2000). Adaptive document image binarization, *Pattern Recognition*, 33(2), 225-236.

[21] Soille P. (2003). *Morphological Image Analysis: Principles and Applications*. (2nd ed.), Springer.

[22] Urcid G., Valdiviezo-N JC., & Ritter GX. (2011). Lattice algebra approach to color image segmentation, *Journal of Mathematical Imaging and Vision*, 42(2-3), 150-162.

[23] Worldwide statistics from breast cancer in BREASTCANCER.org. (2016). [Online] Available: http://www.breastcancer.org/symptoms/understand_bc/statistics.